

The efficiency of star formation in clustered and distributed regions

Ian A. Bonnell^{1*}, Rowan J. Smith^{1,2}, Paul C. Clark², and Matthew R. Bate³

¹ *SUPA, School of Physics and Astronomy, University of St Andrews, North Haugh, St Andrews, Fife, KY16 9SS.*

² *Institut fuer Theoretische Astrophysik, Albert-Ueberle-Str. 2, 69120, Heidelberg, Germany*

³ *School of Physics, University of Exeter, Stocker Road, Exeter, EX4 4QL*

Accepted 0000 December 00. Received 0000 December 00; in original form 0000 October 00

ABSTRACT

We investigate the formation of both clustered and distributed populations of young stars in a single molecular cloud. We present a numerical simulation of a $10^4 M_\odot$ elongated, turbulent, molecular cloud and the formation of over 2500 stars. The stars form both in stellar clusters and in a distributed mode which is determined by the local gravitational binding of the cloud. A density gradient along the major axis of the cloud produces bound regions that form stellar clusters and unbound regions that form a more distributed population. The initial mass function also depends on the local gravitational binding of the cloud with bound regions forming full IMFs whereas in the unbound, distributed regions the stellar masses cluster around the local Jeans mass and lack both the high-mass and the low-mass stars. The overall efficiency of star formation is $\approx 15\%$ in the cloud when the calculation is terminated, but varies from less than 1% in the the regions of distributed star formation to $\approx 40\%$ in regions containing large stellar clusters. Considering that large scale surveys are likely to catch clouds at all evolutionary stages, estimates of the (time-averaged) star formation efficiency for the giant molecular cloud reported here is only $\approx 4\%$. This would lead to the erroneous conclusion of *slow* star formation when in fact it is occurring on a dynamical timescale.

Key words: stars: formation – stars: luminosity function, mass function – globular clusters and associations: general.

1 INTRODUCTION

The ability to conduct wide-area surveys of molecular clouds has shown that most stars form in clusters containing some hundreds to thousands of stars (Lada et al. 1991; Clarke et al. 2000; Lada & Lada 2003). At the same time, mid-infrared surveys such as Spitzer have shown that significant numbers of stars form in a more distributed mode (Allen et al. 2007; Gutermuth et al. 2008, 2009; Evans et al. 2009). The reason why such different modes of star formation exist, and in the same cloud (e.g. Orion A) is unclear.

There has also been considerable interest as to why star formation appears to be inefficient (Evans et al. 2009), with only a few percent of a molecular cloud’s mass being turned into stars per free-fall time. This could imply that star formation is a slow process (Krumholz & Tan 2007) or that it is an inherently inefficient process, but proceeds on the local dynamical timescale. In the latter case the efficiency must increase on small scales where bound clusters are formed.

For example, the Orion Nebula Cluster has a median age of $\approx 10^6$ years and a dynamical time of $\approx 3 \times 10^5$ years (Hillenbrand & Hartmann 1998). Given an overall star formation efficiency of $\approx 50\%$ this implies a star formation per free-fall time of 15%. Considering that the initial pre-cluster cloud is likely to have been at least a factor of 2 larger (Bonnell et al. 2003), this implies an efficiency of star formation per *initial* free-fall time of close to 50 %.

To date, numerical simulations have generally chosen spherically symmetric or period boxes initial conditions of gravitationally bound clouds which collapse and fragment to form stellar clusters (Klessen, Burkert & Bate 1998; Bate, Bonnell & Bromm 2003; Bate 2009). Cluster formation proceeds through hierarchical fragmentation and production of a somewhat distributed population which undergoes a hierachical merger process from small sub-clusters to one final cluster containing most of the stars (Bonnell, Bate & Vine 2003; Bate 2009; Federrath et al. 2010). One simple possibility is that if star formation occurs in regions of molecular clouds that are globally unbound, then there is no reason for the stars that form from the frag-

* E-mail: iab1@st-and.ac.uk

menting population to fall together to form the large stellar cluster. Recent work evaluating the boundness of molecular clouds show that their masses are typically five times smaller than that to be virialised, implying that much of the present day star formation is occurring in unbound molecular clouds(?). Here we demonstrate that the outcome of a distributed or clustered population can depend on whether the region is, or is not, globally bound.

Gravitationally unbound clouds have been explored in a series of studies to investigate how this relates to the efficiency of star formation (Clark & Bonnell 2004; Clark et al. 2005; Clark, Bonnell & Klessen 2008). Low star formation efficiencies are commonly taken to imply that star formation is slow and that molecular clouds are long-lived entities, supported by some internal mechanism and lasting for several tens of dynamical times. In contrast, unbound clouds can also produce low star formation efficiencies on dynamical timescales due to the fact that only a fraction of the cloud becomes gravitationally bound due to the turbulence and undergoes gravitational collapse and star formation.

In this paper, we explore the importance of the local gravitational binding in one cloud and show that a single cloud can produce both a distributed and a clustered population, and a range of star formation efficiencies, depending on the local gravitational binding.

2 CALCULATIONS

The results presented here are based on a large-scale Smoothed Particle Hydrodynamics (SPH) simulation of a cylindrical $10^4 M_{\odot}$ molecular cloud 10 pc in length and 3 pc in cylindrical diameter. We have chosen an elongated cloud rather than the more standard spherical cloud as most molecular clouds are non-spherical and commonly elongated (e.g. Orion A). Such a geometry can also produce additional structure due to gravitational focussing (Hartmann & Burkert 2007). This also allows for the physical properties to be varied along the cloud in a straightforward manner. The cloud has a linear density gradient along its major axis with maximum/minimum values, at each end of the cylinder, 33 percent high/lower than the average gas density of $1.35 \times 10^{-20} \text{ g cm}^{-3}$. The gas has internal turbulence following a Larson-type $P(k) \sim k^{-4}$ power law throughout the cloud and is normalised such that the total kinetic energy balances the total gravitational energy in the cloud. This corresponds to a full cloud (10 pc) 3-D velocity dispersion of order 4.5 km s^{-1} . The density gradient applied then results in one end of the cloud being over bound (still super virial) while the other end of the cloud is unbound.

The cloud is populated with 15.5 million SPH particles on two levels, providing high resolution in regions of interest. We initially performed a lower resolution run with 5 million SPH particles producing an average mass resolution of $0.15 M_{\odot}$ Bate & Burkert (1997). Upon completion of this low resolution simulation, we used three criteria to identify the regions that required higher resolution. This included the particles which formed sinks, and those that were accreted onto sinks. It also included particles which attained sufficiently high density such that their local Jeans mass was no longer resolved in the low-resolution run. All

of these particles were identified and from the initial conditions of the low resolution run, they were split into 9 particles each to create the initial conditions for the high resolution simulations. This particle splitting was performed on the initial conditions to ensure that the physical quantities of mass, momentum, energy and the energy spectrum were preserved. Note that the particle splitting does not introduce finer structure in the turbulent energy spectrum. This produced a mass resolution for the regions involved in star formation of $0.0167 M_{\odot}$, sufficient to resolve the formation of higher-mass brown dwarfs, equivalent to a total number of 4.5×10^7 SPH particles. The equation of state (below) was specified in order to ensure that the Jeans mass in the higher resolution run did not descend below this mass resolution.

Particle splitting results in a marked increase in resolution without unmanageable computational costs (Kitsionas & Whitworth 2002, 2007). Note however some of the unsplit particles, which in the low resolution run neither exceeded their Jeans mass limit nor became involved in the star formation, did get accreted by the additional stars in the high resolution run. This is to be expected as there are now additional locations of star formation not present in the low resolution run and these additional sinks will necessarily accrete unsplit particles.

The simulation follows a modified Larson-type equation of state Larson (2005) comprised of three barotropic equations of state

$$P = k\rho^{\gamma} \quad (1)$$

where

$$\begin{aligned} \gamma &= 0.75; & \rho &\leq \rho_1 \\ \gamma &= 1.0; & \rho_1 < \rho &\leq \rho_2 \\ \gamma &= 1.4; & \rho_2 < \rho &\leq \rho_3 \\ \gamma &= 1.0; & \rho &> \rho_3, \end{aligned} \quad (2)$$

and $\rho_1 = 5.5 \times 10^{-19} \text{ g cm}^{-3}$, $\rho_2 = 5.5 \times 10^{-15} \text{ g cm}^{-3}$, $\rho_3 = 2 \times 10^{-13} \text{ g cm}^{-3}$.

The initial cooling part of the equation of state mimics the effects of line cooling and ensures that the Jeans mass at the point of fragmentation is appropriate for characteristic stellar mass (Jappsen et al. 2005; Bonnell et al. 2006). The $\gamma = 1.0$ approximates the effect of dust cooling while the $\gamma = 1.4$ mimics the effects of an optically thick (to IR radiation) core, although its location at $\rho = 5.5 \times 10^{-15} \text{ g cm}^{-3}$, at lower densities than is typical, is in order to ensure that the Jeans mass is always fully resolved and that a single self-gravitating fragment is turned into a sink particle. A higher critical density for this optically-thick phase where heating occurs would likely result in an increase in the numbers of low mass objects formed. The physical processes described would be unchanged. The final isothermal phase of the equation of state is simply in order to allow sink-particle formation to occur, which requires a subvirial collapsing fragment. The initial conditions of the cloud contain 891 thermal Jeans masses ($M_{\text{Jeans}} \approx 11 M_{\odot}$) such that if the cloud were isothermal, we would expect of order 900 fragments to form.

Star formation in the cloud is modelled through the introduction of sink-particles (Bate, Bonnell & Price 1995). Sink-particles formation is allowed once the gas density of a collapsing fragment reaches $\rho \geq 6.8 \times 10^{-14} \text{ g cm}^{-3}$ although the equation of state ensures that this requires $\rho \geq 2 \times 10^{-13} \text{ g cm}^{-3}$. The neighbouring SPH particles need

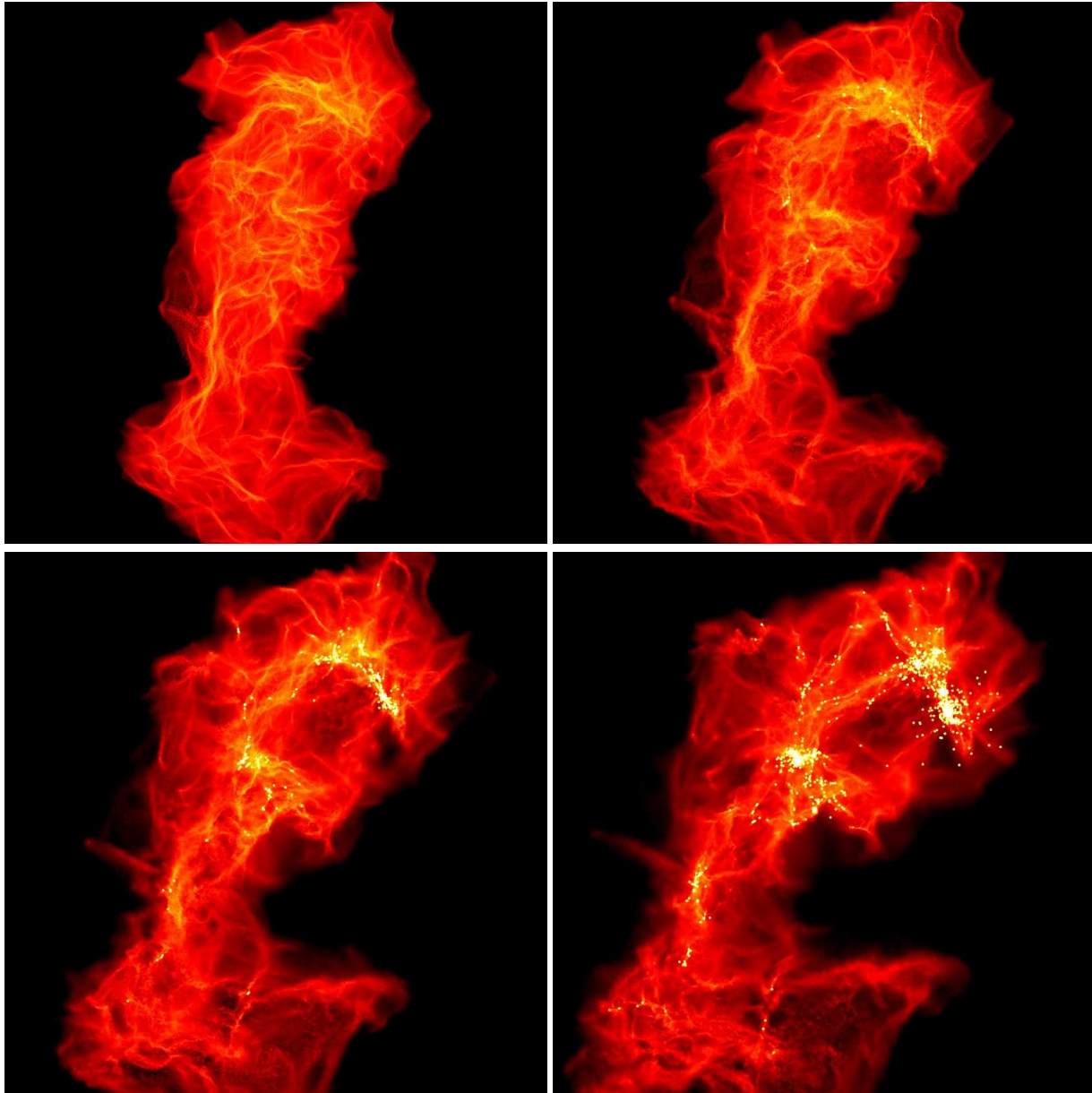


Figure 1. The evolution of our model GMC as it evolves to form both a distributed (bottom) and clustered (top) population of stars. The cloud is initially globally bound but a density gradient along the major axis of the cloud makes the lower region unbound while the top region is gravitationally bound. The cloud is shown at 0.365, 0.544, 0.727 0.961 t_{ff} ($t_{\text{ff}} \approx 6.6 \times 10^5$). Each panel shows the cloud in a 10×10 pc region. The gas column densities are plotted on a logarithmic scale from 0.01 (black) to 100 (white) g cm^{-2} .

be within a radius of $1. \times 10^{-3}$ pc and that fragment must be subvirial and collapsing. Once created, the sinks accrete bound gas within $1. \times 10^{-3}$ pc and all gas that comes within $2. \times 10^{-4}$ pc. The sinks have their mutual gravitational interactions smoothed to $2. \times 10^{-4}$ pc or 40 au. No interactions including binary or disc disruptions can occur within this radius.

We assume a 100 % efficiency of star formation within our sink particles. This likely overestimates the efficiency that would result were feedback from massive stars included. It is worth noting that our gas densities and core sizes are similar to the continuum surveys (Andre ..) that would require a 100 % conversion in order to obtain a mapping from the core mass function to the stellar IMF. Furthermore, Pre-

vious simulations including ionisation and winds (Dale et al. 2005; Dale & Bonnell 2008) do not find a large change in the resultant masses or mass spectra.

3 STAR FORMATION AND THE DEVELOPING IMF

The simulation was followed for 1.02 free-fall times or $\approx 6.6 \times 10^5$ years and $\approx 3.9 \times 10^5$ years after the first stars formed (see Fig. 1). During this time, 2542 stars were formed with masses between 0.017 and $30 M_{\odot}$. The majority of these stars form in the upper gravitationally bound part of the

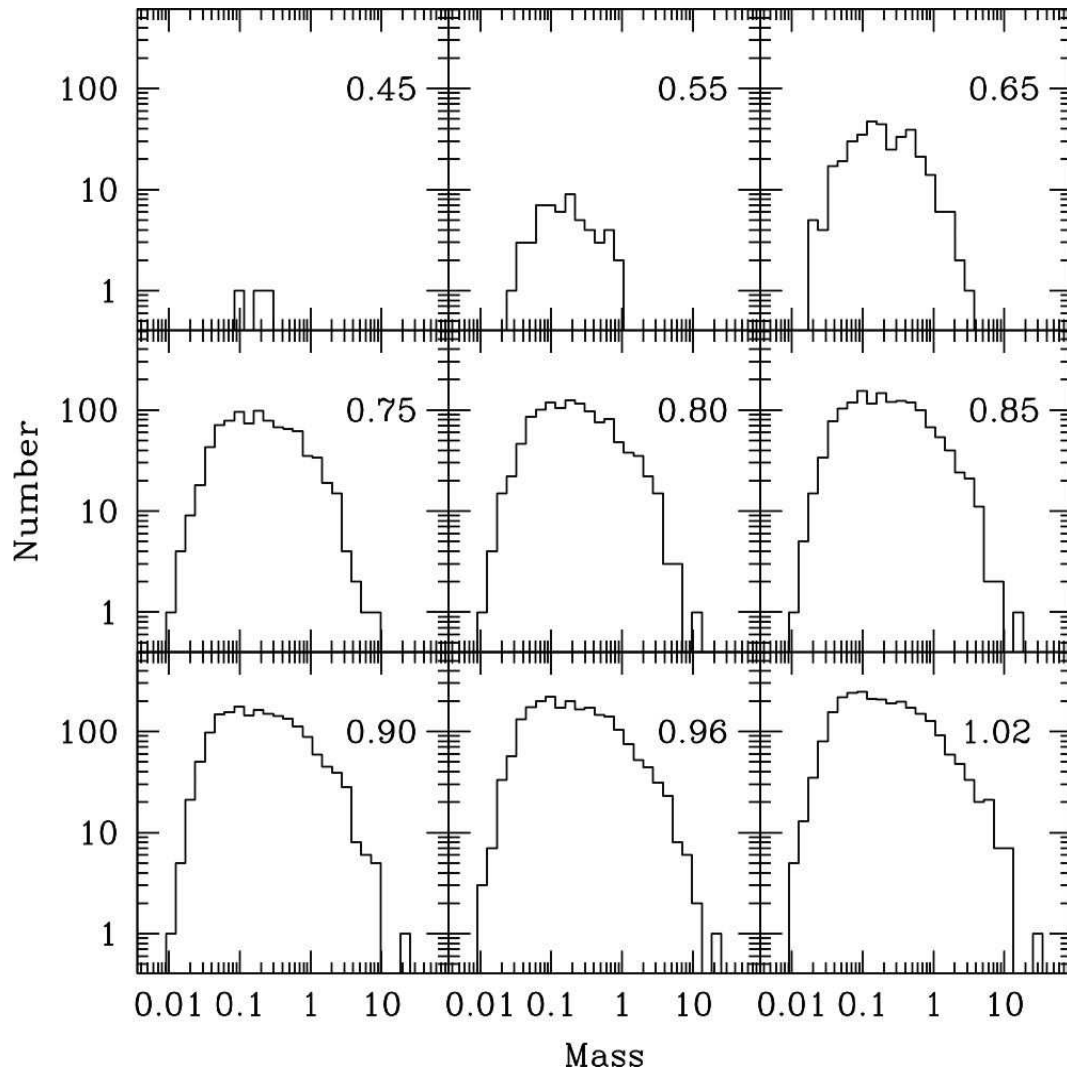


Figure 2. The developing initial mass function of our star forming GC is plotted at various times given in units of the clouds free-fall time, $t_{\text{ff}} \approx 6.6 \times 10^5$.

cloud while some 7 per cent form in the lower, gravitationally unbound regions.

Figure 2 shows the developing initial mass function during the star formation process. The stars form with masses comparable to the Jeans mass of the local gas. These initial masses are initially of the order of several tenths of a Solar mass, while lower mass fragments form stars later in the evolution due to the compression of gas to higher densities as it falls into existing stellar clusters (Bate, Bonnell & Bromm 2002; Bonnell, Clark & Bate 2008). Low and intermediate mass stars located in the centre of forming clusters continue to accreted from the infalling gas and become high-mass stars (e.g. Bonnell, Vine & Bate 2004; Smith, Longmore & Bonnell 2009). This produces a mass function that resembles the stellar IMF at all points during the evolution with a continuous source of low mass stars forming with a decreasing subset of these accreting to ever higher masses. The high-mass end of the IMF is somewhat flatter than Salpeter (Maschberger et al. 2010). This leaves room for the additional physics of feedback from massive stars and the expected decrease in efficiency of mas-

sive star formation. Note that by the massive stars attain their high-mass status through ongoing accretion over relatively long time-periods (Bonnell et al. 2004) such that their feedback could only affect the cloud after much of the star formation has occurred.

The cloud produces a variety of outcomes in terms of the distribution of stellar masses, clustered and distributed modes of star formation as well as the efficiency of the star formation process. These all depend largely on the initial conditions of the cloud and in particular to how gravitationally bound the cloud is locally. The density gradient that is imposed along the major axis, in conjunction with a constant specific kinetic energy of the gas, results in a local variation of the gravitational binding. Measured in terms of the critical mass per unit length to be bound, this variation extends from $M/L = 0.6$ (unbound) to $M/L = 1.4$ (bound with the cloud overall having a $M/L = 1$).

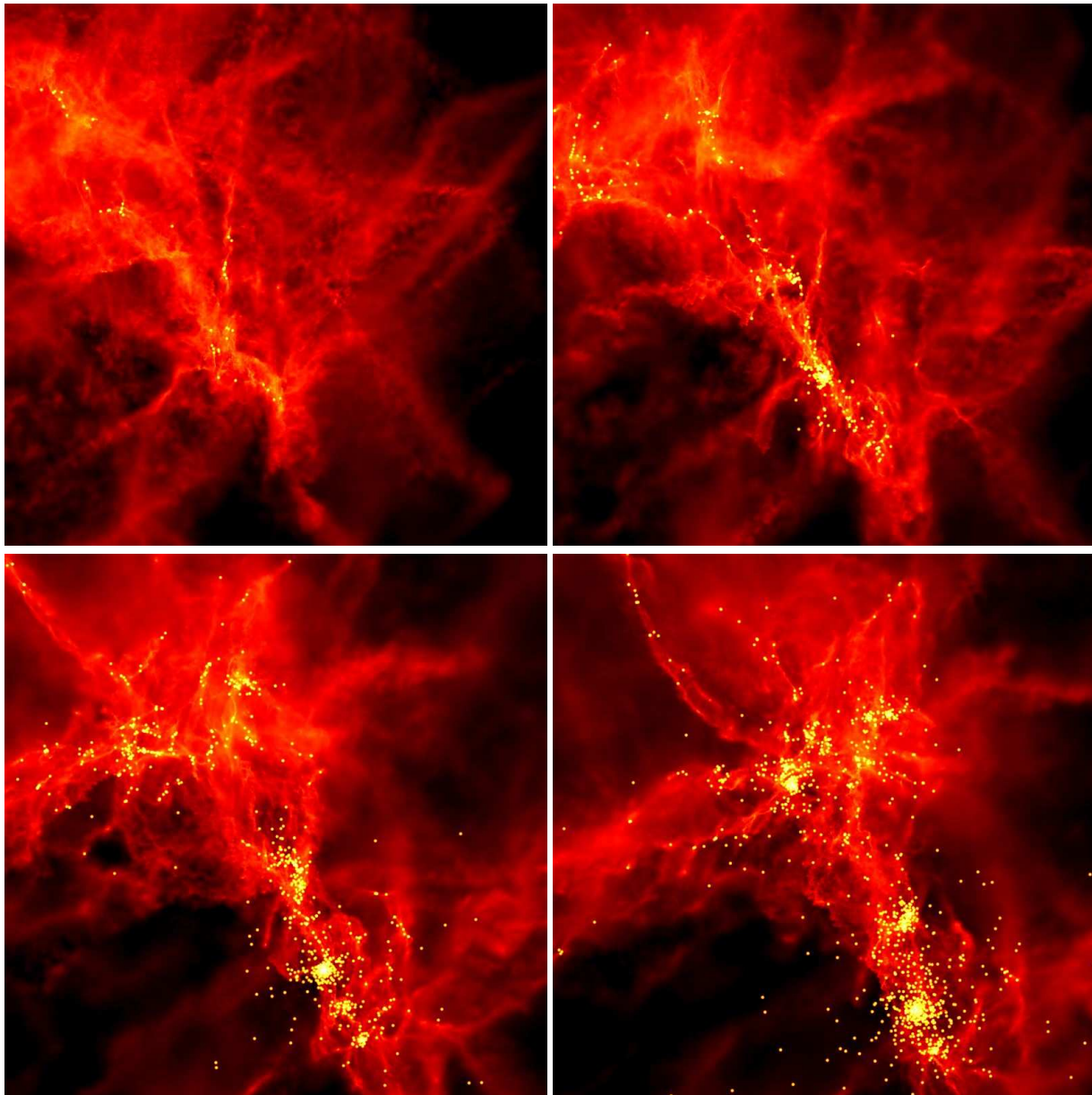


Figure 3. The formation of stellar clusters occurs as infalling gas filaments fragment to form small-N clusters. these clusters grow through the accretion of gas and stars and the merger of subclusters. The cloud is shown at $0.58, 0.73, 0.87$ and $1.02 t_{\text{ff}}$ ($t_{\text{ff}} \approx 6.6 \times 10^5$). Each panel shows the cloud in a $2.0 \times 2.0 \text{ pc}$ region. The gas column densities are plotted on a logarithmic scale from 0.01 (black) to 100 (white) g cm^{-2} .

4 CLUSTERING

The evolution produced a number of high density clusters as well as a distributed population of stars. The clusters form predominantly in the (upper) bound regions of the cloud. The clusters form through the fragmentation of local over-dense filamentary structures that arise due to the turbulence, especially where such filaments intersect. Stars fall into local potential wells and form small-N clusters which quickly grow by accreting other stars (and gas) that flow along the filaments into the cluster potential. The merger of clusters also contributes to the growth of a stellar cluster. Figure 3 shows an example of this process whereby accre-

tion of gas and stars occurs along filaments flowing into the cluster.

An important result from this work is that the clustering depends strongly on the local gravitational binding of the gas prior to star formation. Figure 4 shows the resulting stellar densities as a function of how bound the cloud was initially in terms of the critical mass per unit length, M/L , to be bound. Two measures of the stellar densities are plotted. The blue crosses show the median stellar density determined by the volume needed to contain the ten nearest stellar neighbours. The black triangles show the density of stars contained in a fixed volume of size 0.5 pc . The density determined by the first method is significantly higher as it typically is based on much smaller volumes. In both cases,

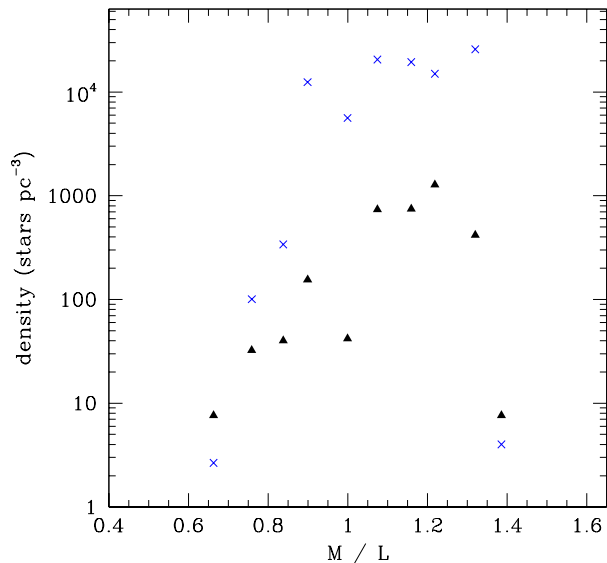


Figure 4. The stellar density is plotted as a function of the local gravitational binding measure in terms of the critical mass to length measure for a cylinder to be gravitationally bound. The higher (blue) points show the median density measured from the ten nearest neighbours to each “star” while the lower value is measure over the local volume of the cloud. We see that low stellar densities correspond to unbound regions of the cloud whereas high stellar densities result from bound regions.

the stellar density is low in regions that were initially unbound and is much higher in the bound parts of the cloud with $M/L > 1$.

This result is understandable in that clusters are (at least temporarily) bound objects and their formation requires that the pre-star formation gas is also bound. In locally unbound regions, it is still possible to form small stellar clusters in regions where turbulent compression and shocks result in a locally bound region. This process is more efficient in regions that are globally bound. Larger scale regions containing many subsystems are bound even before any turbulent support is dissipated. The smaller systems that form locally can then hierarchically merge to form large stellar clusters (Bonnell et al. 2003; Bate 2009). Residual gas in these bound regions then falls into the gravitational potential of the cluster to be competitively accreted by the growing massive stars located in the bottom of the potential well (Bonnell et al. 2004; Bonnell & Bate 2006). The massive stars are thus located in the stellar clusters.

The majority of the stars and brown dwarfs formed are in high-density regions or have been ejected from stellar clusters through interactions (Bate et al. 2002, 2003). As noted in (Bonnell et al. 2008), the brown dwarfs predominantly form in stellar clusters due to the compression of the gas to high local densities as it falls into the gravitational potential. The high-mass stars are also predominantly formed in clusters (Bonnell et al. 2004; Smith et al. 2009). This leads to a potentially observable difference in the stellar IMFs of distributed and clustered star formation. Figure 5 shows the final IMF for the overall population and also for distributed and clustered populations defined as those with a stellar

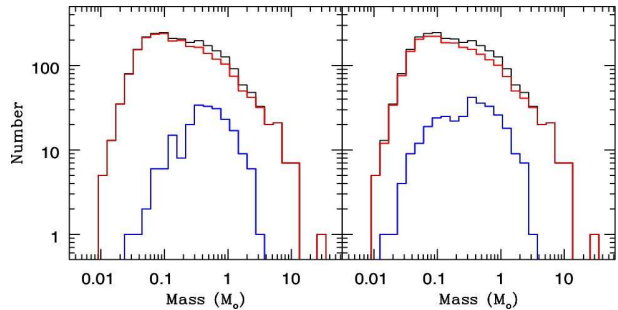


Figure 5. The initial mass functions at the end of the simulation are plotted for the total (top, black line) population and for those stars formed in high-density regions (over 100 stars pc^{-3} , red line) and low density regions (lower, blue line). We see that the low density regions do not form either high or low mass stars and thus result in an unusual IMF. The right hand panel shows the same three distributions but where the stellar density is measured at the end of the simulation. Several stars formed in high-density regions have been ejected from the clusters into the field.

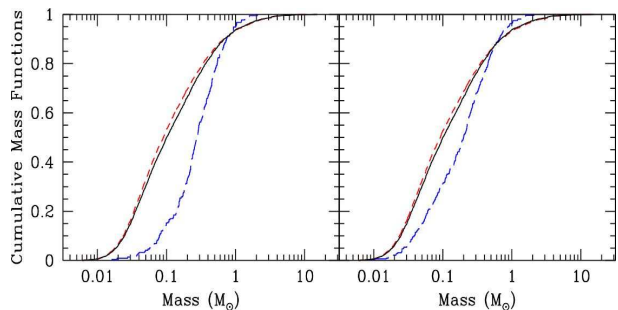


Figure 6. The cumulative mass functions are plotted for the total (solid black line) population and for those stars formed in high-density (over 100 stars pc^{-3} , short-dashed red line) and low density (long-dashed blue line) regions. The right hand panel shows the same three distributions but where the stellar density is measured at the end of the simulation. We see the low-density population is significantly different from that formed in the stellar clusters. This difference remains even after stars are lost from the clusters into the low-density regions.

density lower or higher than 100 stars pc^{-3} . The right-hand panel of figure 5 shows the corresponding populations where they are separated by their maximum stellar density during their evolution. The cumulative distributions (figure 6) show that the two distributions are statistically different and inconsistent (at the 1×10^{-13} level) with being drawn from the same population. The distributed population has a significantly higher median stellar mass and a pronounced lack of low-mass objects. This result helps explain the seemingly anomalous IMF in Taurus which appears to have a lack of brown dwarfs and high-mass stars in a distributed population (Luhman 2004).

5 EFFICIENCY OF STAR FORMATION

One of the central questions we wish to address in this paper is the relationship between the nature and efficiency of the star formation process. Previous studies (i.e. Clark & Bonnell 2004; Clark et al. 2005, 2008) showed that

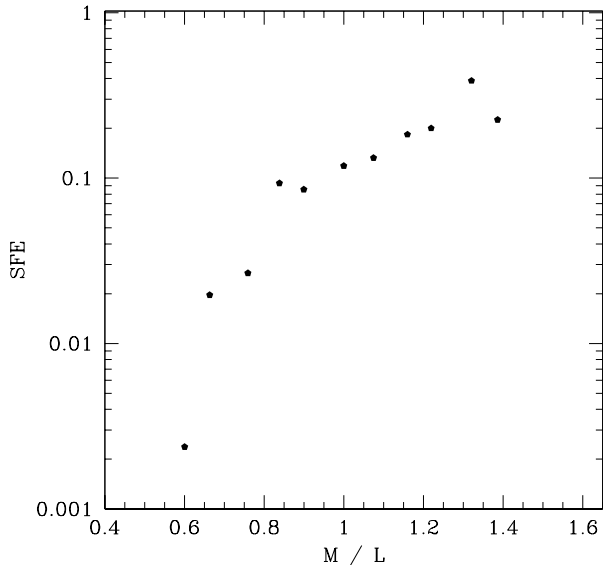


Figure 7. The star formation efficiency is plotted as a function of the critical mass to length ratio for a cylinder to be gravitationally bound. High star formation efficiencies result from very bound regions whereas very low star formation efficiencies result in unbound regions. A mixture of such regions can thus result in the formation of high SFE clustered regions and low SFE distributed populations.

unbound clouds resulted in inefficient star formation. Furthermore, the efficiency reduces dramatically the further the clouds are from being bound. Turbulent compression and shocks results in some star formation in these clouds but it is localised and much of the cloud escapes without entering the star formation process.

In the present study, we have one cloud that has regions which are bound and regions which are unbound with a spatially varying M/L from 0.6 to 1.4. This results in a range in local star formation efficiencies from 0.006 to 0.4. Figure 7 plots the local star formation efficiency as a function of the local binding of the cloud in terms of the critical M/L for the cloud to be globally bound. We see that after 1.02 free-fall times or $\approx 6.6 \times 10^5$ years (and $\approx 3.9 \times 10^5$ years after the first stars formed) the local efficiency of star formation is strongly dependent on local binding of the cloud. The bound regions have efficiencies varying from 10% where the cloud is just bound to 20% for a $M/L = 1.2$ to a peak value of 40% near where the cloud is maximally bound. On the unbound side, the efficiency quickly drops below 10%, reaching values as low as a few % for $M/L < 0.8$. We can thus conclude that small changes in the local binding of the cloud result in vastly different outcomes in terms of the star formation efficiency.

It is worth noting that there is a strong correlation between the local efficiency of star formation and the formation of stellar clusters. Regions with relatively high efficiencies of $\geq 10\%$ corresponds to regions which are bound and thus form stellar clusters. In contrast the unbound regions form a relatively distributed, low stellar density population and does so at very low efficiencies. This is in agreement with observations where clustered regions are found to have higher

star forming efficiencies, whereas distributed regions such as Taurus have low star formation efficiencies. These differences in the star formation efficiencies reported here are not simply due to delays in star formation in the unbound parts of the cloud as most of the mass is actually leaving the cloud and cannot partake in the star formation process (Clark et al. 2008).

6 OBSERVABLE DETERMINATION OF THE STAR FORMATION EFFICIENCY

The evolution of the star formation efficiency is shown in figure 8 from where the first stars form at $t \approx 0.5t_{\text{ff}}$ to the end of the simulation at $t \approx 1.0t_{\text{ff}}$. The overall star formation efficiency as measured at the end of the simulation is $\approx 15\%$. this global value is an upper limit as no feedback effects are included (e.g. Dale & Bonnell 2008). Magnetic fields could also act to reduce this number further (Price & Bate 2008, 2009). For example, if feedback acted to destroy the cloud at $0.7t_{\text{ff}}$, then the final star formation efficiency would be of order 5%.

Such global star formation efficiencies are commonly invoked to discriminate between *slow*, and *fast* star formation. Slow star formation invokes some supporting mechanism to prolong the lifetime of molecular clouds to many tens of dynamical times (Krumholz & Tan 2007) whereas fast star formation is expected to occur on timescales of several dynamical times (Elmegreen 2000). Comparing such ideas to observations of large scale star formation rates can be problematic as we do not know if the measured star formation efficiencies are final, intermediate or even pre-star formation values. Figure 8 also shows the time averaged star formation efficiency at any given time during the cloud’s evolution. This takes into account that when measuring global volume averaged values, we are just as likely to observe any particular cloud at any point in its evolution. The time averaged star formation efficiency is significantly lower than the instantaneous value throughout its evolution, due to the amount of time the cloud spends in its pre-star formation stage. This neglects the time take for the cloud to form which should be of order or greater than the dynamical time of the cloud. Nevertheless, the final time-averaged star formation efficiency is $\approx 3 - 4\%$. So, in a volume where a mixture of clouds of different evolutionary stages are present, an observer would estimate star formation efficiency of several percent and thus conclude that this was *slow* star formation, when in reality star formation is locally proceeding on a dynamical timescale. All of the above neglects the effects of magnetic fields and feedback which both act to reduce the star formation rates and efficiencies. While magnetic fields do slow down star formation (Price & Bate 2008, 2009), feedback impedes or locally stops star formation without appreciably changing its dynamical nature (Dale et al. 2005; Dale & Bonnell 2008)

7 DISCUSSION: THE EVOLUTION OF GIANT MOLECULAR CLOUDS

We have seen from the above that low star formation efficiencies are plausibly due to the GMCs not being com-

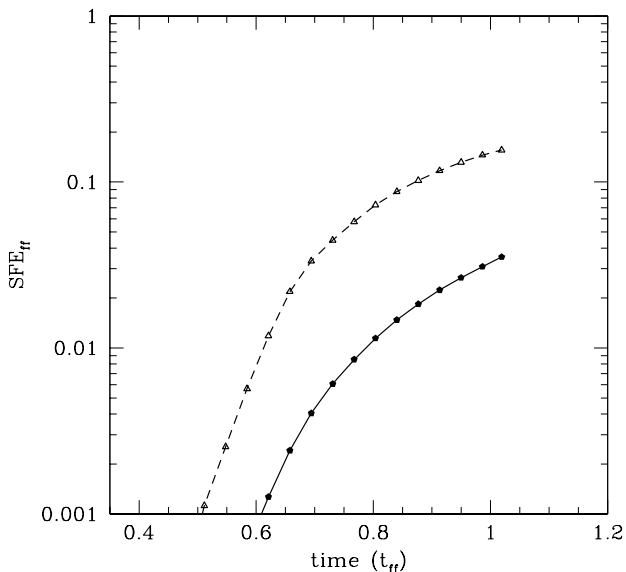


Figure 8. The total (dashed) and time-averaged (solid) star formation efficiencies are plotted as a function of time. While the final instantaneous SFE is of order 15 %, an observer detecting a full population of such clouds would likely sample all evolutionary stages and thus measure the much lower time-averaged star formation efficiency of $\approx 4\%$.

pletely bound by their self gravity. Even in the absence of effects such as magnetic fields and feedback, clouds that are globally, or at least in large part unbound result in low star formation efficiencies. Star formation requires that the clouds are nearly bound or at least have significant regions which are close to being bound, with typically gravitational and kinetic energies within a factor of a few of each other (Clark, Bonnell & Klessen 2008). From this starting point, we can try to construct an evolutionary scenario for GMCs in which self-gravity only plays a role in the actual star formation process (Pringle et al. 2001; Bonnell et al. 2006; Dobbs et al. 2006). We will neglect the effects of the magnetic field but to first order its effects would be to increase the internal energy of the clouds such that they are further from being gravitationally bound.

The formation of giant molecular clouds is uncertain with various theories from gravitational instabilities to cloud coagulation and spiral shocks (McKee & Ostriker 2007). In reality all of these processes may play a significant role in GMC formation but for our purposes, we will assume that GMC formation occurs primarily due to spiral shocks or cloud coagulations (Dobbs et al. 2006). In such cases, self-gravity need not play an important role in the formation process and clouds can be formed without being gravitationally bound.

Cloud formation from external collisions or compression implies an increasing contribution to the cloud’s gravitational potential. During formation, the cloud evolves from a state where self-gravity is unimportant to one where self-gravity has a significant effect on the cloud’s dynamics. Once the gravitational energy is within a factor of a few of the kinetic energy, then star formation proceeds in local regions that become bound due to the cloud’s internal dynamics

(Clark, Bonnell & Klessen 2008). This local star formation will occur as parts of the cloud are still being assembled as the local timescale is much shorter than the overall dynamical time for the cloud or its precursor.

Star formation would then proceed until either the local gas reservoir is depleted, or until the gas reservoir is removed by the effects of feedback from young stars. The tidal shear from leaving the spiral arm potential could also limit the lifetime of the clouds (Dobbs et al. 2006). The majority of the cloud need never become gravitationally bound before the cloud is dispersed resulting in inefficient star formation process that is still occurring on a fast dynamical timescale.

8 CONCLUSIONS

Star formation in realistic GMCs will proceed from a variety of physical conditions, spanning regions that are gravitationally bound to parts or whole clouds which are gravitationally unbound. Star formation will occur as long as the local conditions are close to being gravitationally bound but the properties of the young stellar population can depend strongly on these conditions. Regions that are bound produce bound stellar clusters and a stellar population that follows the full initial mass function from brown dwarfs to high-mass stars. Regions that are unbound are likely to produce a somewhat skewed IMF biased towards the local Jeans mass in the gas and with significant lack of lower-mass stars, such as is seen in Taurus (Luhman 2004).

The star formation efficiency is also a product of the local physical conditions with bound regions resulting in a relatively high star formation efficiency of order 10 % or more per free-fall time. Regions that are unbound can have drastically reduced efficiencies of order 1 % or less per free-fall time. Thus clustered star formation should occur in regions of higher local star formation efficiencies that more distributed populations.

Estimates of low star formation efficiencies are equally consistent with fast dynamical star formation as slow quasistatic star formation provided that one relaxes the condition that GMCs are globally bound long-lived entities. Including the pre-star formation timeperiods where clouds are being assembled, global estimates of depletion timescales or star formation rates per free-fall time will appear to be low even while local regions are undergoing fast star formation at high efficiencies.

Finally, realistic GMCs are likely to be constructed from a mix of physical conditions such that a fraction of the cloud is bound producing stellar clusters at high efficiencies whereas the majority of the cloud is unbound producing a more distributed population at low star formation efficiencies before the cloud is unbound by feedback or alternative process. Such a scenario is consistent with a model where GMCs are not formed due to their self-gravity but rather to an external process such as spiral shocks (Dobbs et al. 2006; Dobbs 2008).

ACKNOWLEDGMENTS

We acknowledge the contribution of the U.K. Astrophysical Fluids Facility (UKAFF) and SUPA for providing the

computational facilities for the simulations reported here. IAB thanks the ETCC committee of STFC for providing the rail journeys on which this paper was written. PCC acknowledges support by the Deutsche Forschungsgemeinschaft (DFG) under grant KL 1358/5 and via the Sonderforschungsbereich (SFB) SFB 439, Galaxien im frühen Universum. MRB is grateful for the support of a Philip Leverhulme Prize and a EURYI Award. This work, conducted as part of the award ‘The formation of stars and planets: Radiation hydrodynamical and magnetohydrodynamical simulations’ made under the European Heads of Research Councils and European Science Foundation EURYI (European Young Investigator) Awards scheme, was supported by funds from the Participating Organizations of EURYI and the EC Sixth Framework Programme. We would like to thank Chris Rudge and Richard West at the UK Astrophysical Fluid Facility (UKAFF) for their tireless assistance and enthusiasm during the completion of this work.

REFERENCES

- Allen L., Megeath S. T., Gutermuth R., Myers P. C., Wolk S., Adams F. C., Muzerolle J., Young E., Pipher J. L., 2007, *Protostars and Planets V*, pp 361–376
- Bate M. R., 2009, *MNRAS*, 392, 590
- Bate M. R., Bonnell I. A., Bromm V., 2002, *MNRAS*, 332, L65
- Bate M. R., Bonnell I. A., Bromm V., 2003, *MNRAS*, 339, 577
- Bate M. R., Bonnell I. A., Price N. M., 1995, *MNRAS*, 277, 362
- Bate M. R., Burkert A., 1997, *MNRAS*, 288, 1060
- Bonnell I. A., Bate M. R., 2006, *MNRAS*, 370, 488
- Bonnell I. A., Bate M. R., Vine S. G., 2003, *MNRAS*, 343, 413
- Bonnell I. A., Clark P., Bate M. R., 2008, *MNRAS*, 389, 1556
- Bonnell I. A., Clarke C. J., Bate M. R., 2006, *MNRAS*, 368, 1296
- Bonnell I. A., Dobbs C. L., Robitaille T. P., Pringle J. E., 2006, *MNRAS*, 365, 37
- Bonnell I. A., Vine S. G., Bate M. R., 2004, *MNRAS*, 349, 735
- Clark P. C., Bonnell I. A., 2004, *MNRAS*, 347, L36
- Clark P. C., Bonnell I. A., Klessen R. S., 2008, *MNRAS*, 386, 3
- Clark P. C., Bonnell I. A., Zinnecker H., Bate M. R., 2005, *MNRAS*, 359, 809
- Clarke C. J., Bonnell I. A., Hillenbrand L. A., 2000, *Protostars and Planets IV*, pp 151–+
- Dale J. E., Bonnell I. A., 2008, *MNRAS*, 391, 2
- Dale J. E., Bonnell I. A., Clarke C. J., Bate M. R., 2005, *MNRAS*, 358, 291
- Dobbs C. L., 2008, *MNRAS*, 391, 844
- Dobbs C. L., Bonnell I. A., Pringle J. E., 2006, *MNRAS*, 371, 1663
- Elmegreen B. G., 2000, *MNRAS*, 311, L5
- Evans N. J., Dunham M. M., Jørgensen J. K., Enoch M. L., Merín B., van Dishoeck E. F., Alcalá J. M., Myers P. C., 2009, *ApJS*, 181, 321
- Federrath C., Banerjee R., Clark P. C., Klessen R. S., 2010, *ApJ*, 713, 269
- Gutermuth R. A., Megeath S. T., Myers P. C., Allen L. E., Pipher J. L., Fazio G. G., 2009, *ApJS*, 184, 18
- Gutermuth R. A., Myers P. C., Megeath S. T., Allen L. E., Pipher J. L., Muzerolle J., Porras A., Winston E., Fazio G., 2008, *ApJ*, 674, 336
- Hartmann L., Burkert A., 2007, *ApJ*, 654, 988
- Hillenbrand L. A., Hartmann L. W., 1998, *ApJ*, 492, 540
- Jappsen A.-K., Klessen R. S., Larson R. B., Li Y., Mac Low M.-M., 2005, *A&A*, 435, 611
- Kitsionas S., Whitworth A. P., 2002, *MNRAS*, 330, 129
- Kitsionas S., Whitworth A. P., 2007, *MNRAS*, 378, 507
- Klessen R. S., Burkert A., Bate M. R., 1998, *ApJ*, 501, L205+
- Krumholz M. R., Tan J. C., 2007, *ApJ*, 654, 304
- Lada C. J., Lada E. A., 2003, *ARA&A*, 41, 57
- Lada E. A., Depoy D. L., Evans II N. J., Gatley I., 1991, *ApJ*, 371, 171
- Larson R. B., 2005, *MNRAS*, 359, 211
- Luhman K. L., 2004, *ApJ*, 617, 1216
- Maschberger T., Clarke C. J., Bonnell I. A., Kroupa P., 2010, *MNRAS*, 404, 1061
- McKee C. F., Ostriker E. C., 2007, *ARA&A*, 45, 565
- Price D. J., Bate M. R., 2008, *MNRAS*, 385, 1820
- Price D. J., Bate M. R., 2009, *MNRAS* submitted, 0
- Pringle J. E., Allen R. J., Lubow S. H., 2001, *MNRAS*, 327, 663
- Smith R. J., Longmore S., Bonnell I., 2009, *MNRAS*, 400, 1775

This paper has been typeset from a \TeX / \LaTeX file prepared by the author.